Research Square

Preprints are preliminary reports that have not undergone peer review.
They should not be considered conclusive, used to inform clinical practice,
or referenced by the media as validated information.

Mechanical response and precursor characteristics of catastrophic failure in deep coal mass with through-openings : Insights from experiments

Ji Ma

showsma@hpu.edu.cn

Henan Polytechnic University

Zhouyang Jiang

Henan Polytechnic University

Housheng Jia

Henan Polytechnic University

Ruifu Yuan

Henan Polytechnic University

Zhiqiang Hou

Henan Polytechnic University

Lifang Feng

Henan Polytechnic University

Zhengxuan Yang

Henan Polytechnic University

Xiao Li

Zhongye Changtian International Engineering Co.,Ltd

Research Article

Keywords: Deep coal mass, Catastrophic failure, Opening geometry, Power-law acceleration, Critical slowing-down

Posted Date: September 9th, 2026

DOI: https://doi.org/10.21203/rs.3.rs-10829244/v1

License: This work is licensed under a Creative Commons Attribution 4.0 International License.
Read Full License

Additional Declarations: No competing interests reported.

Mechanical response and precursor characteristics of catastrophic failure in deep coal mass with through-openings : Insights from experiments

Ji Ma[a,b,e,*], Zhouyang Jiang[c], Housheng Jia[a,b], Ruifu Yuan[a,d], Zhiqiang Hou[a,b], Lifang Feng[c], Zhengxuan Yang[c], Xiao Li[f]

a School of Energy Science and Engineering, Henan Polytechnic University, Jiaozuo 454003, China;
b Synergism Innovative Center of Coal Safety Production in Henan Province, Jiaozuo 454000, China;
c School of Safety Science and Engineering, Henan Polytechnic University, Jiaozuo 454003, China;
d Zhengzhou Institute for Advanced Research of Henan Polytechnic University,Zhengzhou 451464, China;
e State and Local Joint Engineering Laboratory for Gas Drainage & Ground Control of Deep Mines, Henan Polytechnic University, Jiaozuo 454000, China;
f Zhongye Changtian International Engineering Co.,Ltd, Changsha 410205, China.
*E-mail address of the corresponding author Ji Ma: showsma@hpu.edu.cn.

Abstract

To clarify how opening geometry affects precursory characteristics of catastrophic failure in deep roadways, constrained uniaxial compression tests were conducted on intact coal and specimens with circular, arched, square, or trapezoidal through-openings. Acoustic emission (AE) and digital image correlation (DIC) were used to monitor strain and AE signals during loading. Critical power-law exponents and critical-slowing-down indicators were derived from strain-rate and AE-rate series, with trend significance and robustness checked via the Mann-Kendall test and a parameter-sensitivity analysis. All five groups showed accelerating strain-rate and AE-rate responses before failure, with group-mean critical power-law exponents ranging from -0.65 to -0.98. Strain-rate acceleration was strongest for trapezoidal and square openings, whereas AE-rate acceleration peaked for circular openings, reflecting different sensitivities of strain localization and microcracking to opening geometry. Critical-slowing-down precursors appeared at t/t_f = 0.78-0.91, with AE-rate precursors generally preceding strain-rate ones; the rising variance was more significant and robust than the rising autocorrelation coefficient. The two precursors respectively mark the

transition from stable damage accumulation to accelerated propagation and the divergence of response rates near failure, thus complementing each other across time scales. A dual-timescale prediction strategy is proposed: a sustained significant variance increase triggers early risk identification, and stable power-law acceleration in strain or AE rate confirms imminent failure. These results support multisource monitoring and tiered early warning of catastrophic failure in deep coal with through-openings.

Keywords

Deep coal mass; Catastrophic failure; Opening geometry; Power-law acceleration; Critical slowing-down

1 Introduction

With the increasing depth of coal mining, dynamic disasters such as rock bursts and large deformations of surrounding rock in roadways have become increasingly frequent and severe (He et al. 2023a; He et al. 2023b; Ren et al. 2025; Xie et al. 2018; Ma et al. 2023; Kong et al. 2025). The essence of these dynamic disasters lies in the catastrophic failure of the roadway surrounding rock (Dai et al. 2021; Fan et al. 2020), and such catastrophic failure is typically characterized by its mechanical properties and behaviors (Zhang et al. 2021). Therefore, revealing the precursory mechanical responses of roadway surrounding rock before catastrophic failure is fundamental for achieving effective early warning and prediction.

In brittle media, the response variables exhibit power-law singularity before catastrophic failure, which is a typical physical precursor (Hao et al. 2013; Xue et al. 2018; Fan et al. 2024; Zhang et al. 2023). Specifically, variables such as the AE event rate (Zhai et al. 2021; Niu and Zhou 2021; Zhou and Li 2022; Zhang et al. 2025a), AE hit rate (Zhang et al. 2023), horizontal strain (Cheng et al. 2024a), strain rate (Cheng et al. 2024b; Huang et al. 2025; Ma et al. 2025), and strain acceleration (Cheng et al. 2024b; Cheng et al. 2024c) all display power-law characteristics before failure, and such power-law behavior has been explained by mesoscopic damage mechanics (Tang and Zhu 2020). Rock tests have shown that the power-law exponents of strain, AE event rate, and related response variables evolve as failure approaches (Hao et al. 2013; Xue et al. 2018; Niu and Zhou 2021; Zhang and Zhou 2020). DIC results further indicate

that strain acceleration exhibits significant spatial heterogeneity and is controlled by the location of the localization band and the monitoring scale (Cheng et al. 2024b); the predictability of AE acceleration also depends on the crack process zone and material heterogeneity (Zhang et al. 2023; Vasseur et al. 2015). Consequently, the critical exponents derived from a single measurement point or a single response variable may be affected by the localized deformation path around the opening. Although relying solely on the imminent failure power-law acceleration is helpful for pinpointing the failure time, its effective window is generally short.

The critical slowing-down phenomenon occurs before a state transition in a dynamical system; it refers to increased fluctuation amplitude and persistence, weakening of recovery capability near the critical point (Zhu et al. 2025). Generally, increases in the autocorrelation coefficient and variance are considered indicators that the system is approaching a critical point. For sandstone and granite, the autocorrelation coefficient and variance of AE parameters increase sharply before critical fracture (Zheng et al. 2025; Wang et al. 2024); the sudden significant increase in the autocorrelation coefficient and variance of AE counts can serve as precursor for sandstone specimens failure (Wei et al. 2018). Moreover, the autocorrelation coefficient exhibits greater fluctuations than the variance (Li et al. 2023); using variance to identify early warning signals is easier and more reliable than using the autocorrelation coefficient, and the characteristics of warning signals are closely related to the inherent properties of the rock and external testing conditions (Zhang et al. 2021b). The precursor time calculated from the critical slowing-down of AE amplitude in slate and mica schist is earlier than that obtained directly from AE parameters, effectively improving the warning time and offering higher sensitivity (Zhu et al. 2025). Studies on shale show that early warning based on the autocorrelation coefficient can provide a warning, while that based on variance can provide short-term warning (Yang et al. 2024). Some research combined statistical methods with AE parameters and found that precursors from critical slowing-down theory appear earlier than those from the b-value and information entropy, whereas precursors from the Mann–Kendall (M–K) test are the latest, which can serve as long-term and short-term warning precursors, respectively

(Ling et al. 2025). Additionally, the coal infrared-radiation (Hao et al. 2022) and AE-energy (Kong et al. 2023) sequences analyzed using critical-slowing-down theory can also provide early warnings for coal–rock dynamic disasters.

Existing studies have mostly examined power-law acceleration or critical slowing-down separately, and they often focus on a single lithology, a single opening shape, or a single monitoring variable. For complete coal and coal with different through-openings, the following knowledge is still lacking: whether the strain rate and AE rate share a common power-law regime in the imminent failure stage; how the opening geometry alters the similarity and difference between the strain rate and AE rate; whether the precursor timing, stress level, significance, and parameter robustness of critical slowing-down follow consistent patterns; and whether the two precursors can form a temporally complementary hierarchical warning chain.

To this end, this paper conducts confined uniaxial compression tests on complete coal specimens and coal specimens with four different through-openings, and simultaneously acquires DIC strain and AE data. First, we compare the stage evolution of strength, characteristic stresses, and response rates; then we extract the critical power-law exponents of the two response variables and analyze intra-group coupling and inter-group differences. Further, we identify critical slowing-down based on the variance and autocorrelation coefficient of detrended sequences, and evaluate their reliability using the Mann–Kendall test and parameter sensitivity analysis. Finally, we clarify the physical connection between the two precursors and propose a dual-timescale prediction strategy that balances advance warning and imminent-failure accuracy.

2 Experimental procedure and data preprocessing

2.1 Specimens and testing system

The specimens were taken from the same coal seam of the Shicaocun Coal Mine in Ningxia (Figure 1(a)), at a depth of 700–800 m. The coal exhibited strong rockburst proneness. All coal specimens were cored perpendicular to the bedding direction and machined into rectangular prismatic specimens of approximately 50 × 50 × 100 mm. On this basis, one group of circular through-openings with a diameter of 10 mm was

drilled at the center of the specimens, and three additional groups contained arched, square, and trapezoidal through-openings, each inscribed within a circle of 10 mm diameter; one group of complete specimens without through-openings was retained as a control. Seven specimens were prepared for each group, and the end-face flatness error was controlled within 0.02 mm, meeting the requirements for rock mechanics testing. The geometric areas of the circular, arched, square, and trapezoidal openings were 78.54, 55.02, 49.98, and 47.71 mm², respectively. Detailed geometric parameters are shown in Figure 1(b).

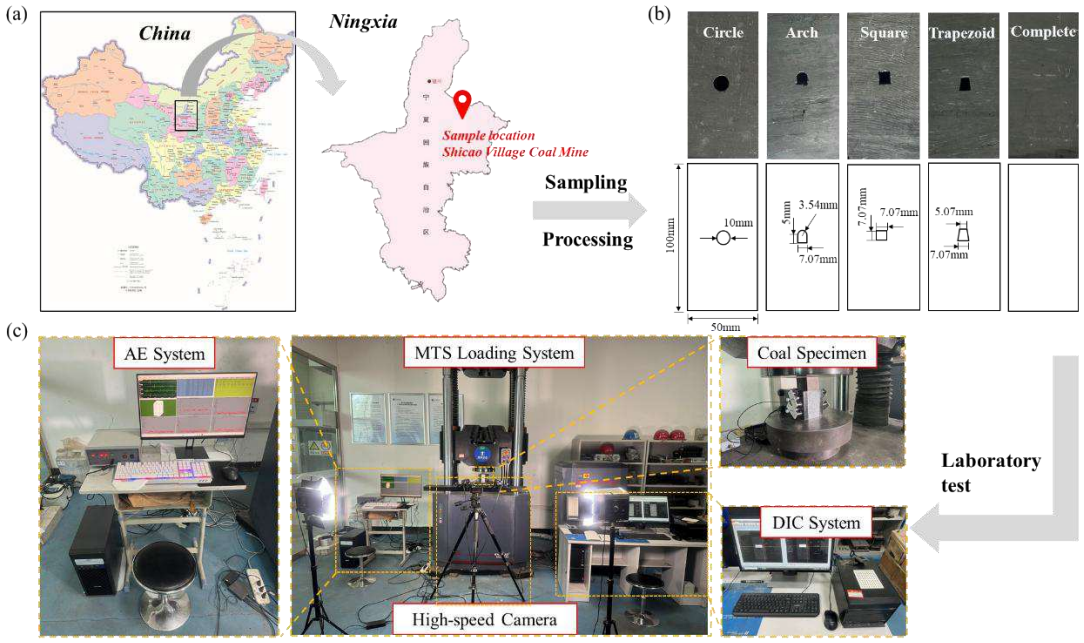


Figure 1. Sampling location, specimen dimensions, and experimental system: (a) sampling location; (b) dimensional parameters of coal specimens; (c) experimental system

The experimental system consists of three subsystems: loading, acoustic emission (AE), and digital image correlation (DIC). Axial loading was applied using an MTS-2000 computer-controlled electro-hydraulic servo universal testing machine, with a maximum load capacity of 2000 kN. The AE system comprised an acquisition unit (DS5-8A), four sensors, and four preamplifiers. Two sensors were mounted on each of the left and right lateral sides of the specimen to continuously monitor crack activity during the loading process. Strain on the specimen was acquired by the DIC system, which consisted of a high-speed camera, two light sources, and MatchID software. The overall layout of the experimental system is shown in Figure 1(c).

2.2 Experimental scheme

To approximately simulate the confined deformation environment of deep roadway surrounding rock, the upper crossbeam of the testing machine was kept fixed during the tests. The left, right, and rear lateral sides of the specimen were restrained by fixtures, and a spacer block was placed on the top of the specimen to improve load transfer uniformity and reduce end effects. Loading was applied under displacement control, achieved by the actuator outputting a monotonically increasing displacement. The axial load applied to the specimen was acquired via a load cell mounted on the loading plate of the testing machine. The lower loading plate of the testing machine moved upward at a constant rate of 0.005 mm/s. The AE sampling rate was set to 3 MHz, and the threshold was set at 40 dB. The high-speed camera was positioned in front of the specimen and operated at 8 fps. All acquisition systems were synchronously triggered to ensure a unified time reference for the stress, strain, and AE sequences.

3 Results

3.1 Strength characteristic analysis

Figure 2(a) shows that the uniaxial compressive strength (UCS) of coal specimens with different opening shapes exhibits a relatively low overall scatter, with most test values lying within one standard deviation of the group mean. Therefore, the group mean adequately represents the strength level of each geometry. The opening area influenced the group-mean UCS of the coal specimens: except for the arched-opening coal specimens, the mean UCS of the remaining coal specimens gradually increases with decreasing opening area (the complete coal specimens are considered as having zero opening area). Although the opening area of the arched-opening coal specimens is second only to that of the circular-opening specimens, their mean UCS is the highest among all opening-containing specimens, indicating that the opening shape also significantly affects the mean UCS. Overall, the mean UCS of the five types of coal specimens, from lowest to highest, follows the order: circular opening, square opening, trapezoidal opening, arched opening, and complete specimen. The complete specimens exhibit the highest mean UCS, while the introduction of internal openings generally leads to strength reduction, with the circular-opening specimens experiencing the

largest strength decrease.

Using the mean UCS of the complete specimens as a baseline, the strength deterioration coefficient η is defined as the ratio of the mean UCS of the opening-containing specimens to that of the complete specimens. A smaller η indicates a more significant weakening effect of the opening on the coal strength. The η values for the circular, arched, square, and trapezoidal opening specimens are 0.73, 0.98, 0.83, and 0.96, respectively. That is, the mean UCS of the circular-opening specimens decreases by approximately 27% compared with the complete specimens. This phenomenon may originate from the tendency of a uniform and symmetrical stress concentration zone to form around the circular opening; this symmetric stress field facilitates coupling between the maximum tensile stress zone around the opening and the randomly distributed weak pre-existing weak fissures within the coal, thereby rapidly inducing dominant cracks and leading to sudden overall instability at a low stress level. In contrast, the mean UCS of the arched-opening specimens is only about 2% lower than that of the complete specimens and about 33% higher than that of the circular-opening specimens, reflecting the combined effect of load transfer through the arch crown and energy dissipation caused by localized damage along the straight sidewalls. The square-opening and trapezoidal-opening specimens have mean UCS values between those of the arched-opening and circular-opening groups, being approximately 12% and 31% higher than the circular-opening group, respectively. The reason may be that extremely high stress concentrations occur at the sharp corners of the square and trapezoidal openings, causing local crushing or generating numerous microcracks at relatively low loads. Such local damage consumes additional energy and disturbs the original stress field around the opening, delaying the initiation of the main crack and making its propagation path more complex; therefore, a higher load is required to trigger overall failure. In other words, compared with the circular opening, the trapezoidal and square openings with angular corners alter the stress concentration distribution and crack propagation path, thereby enhancing the uniaxial compressive strength of the coal specimens.

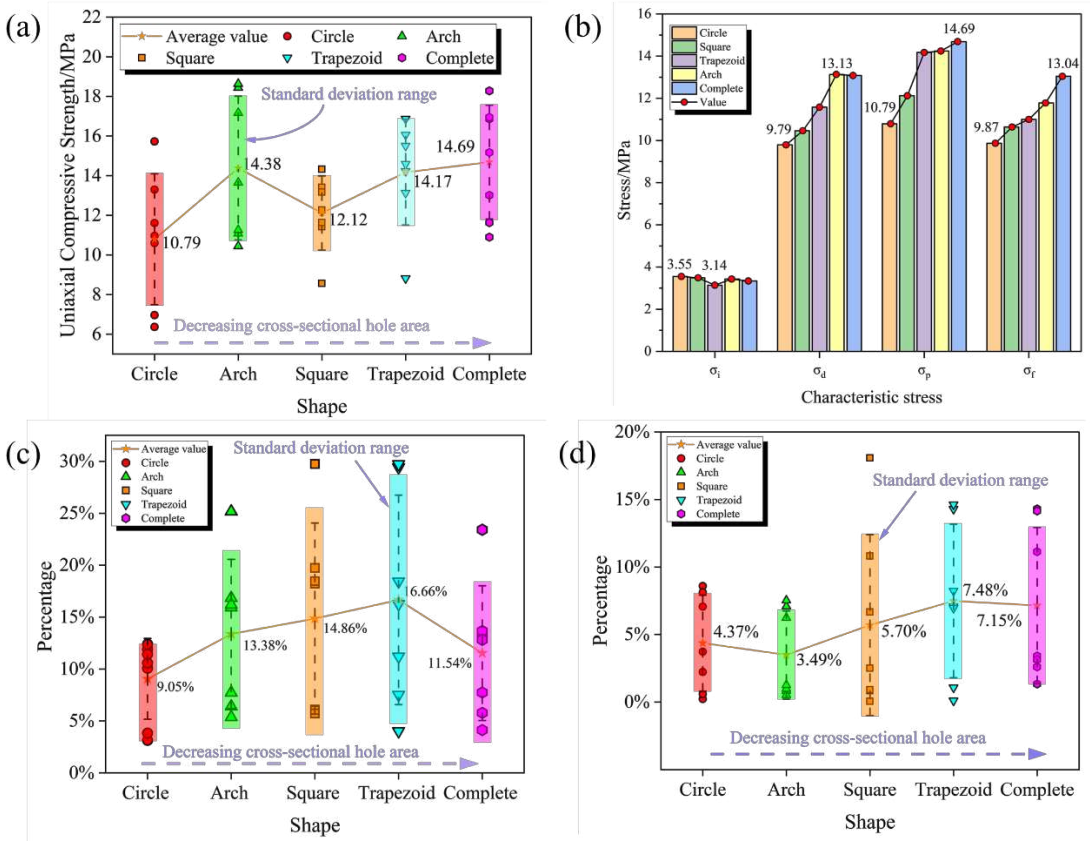


Figure 2. Strength and dispersion characteristics of coal specimens with different opening shapes: (a) uniaxial compressive strength; (b) mean characteristic stresses; (c) percentage duration of the metastable stage (III); (d) percentage duration of the sub-instability stage (IV)

3.2 Evolution of mechanical response variables

To ensure that the subsequent analyses of mechanical response, surface strain field, and macroscopic failure morphology are representative, one specimen with the UCS closest to the group mean was selected from each group of seven specimens as a representative specimen. This selection was intended to best represent the common mechanical response of each opening geometry and to reduce the influence of inter-specimen variability.

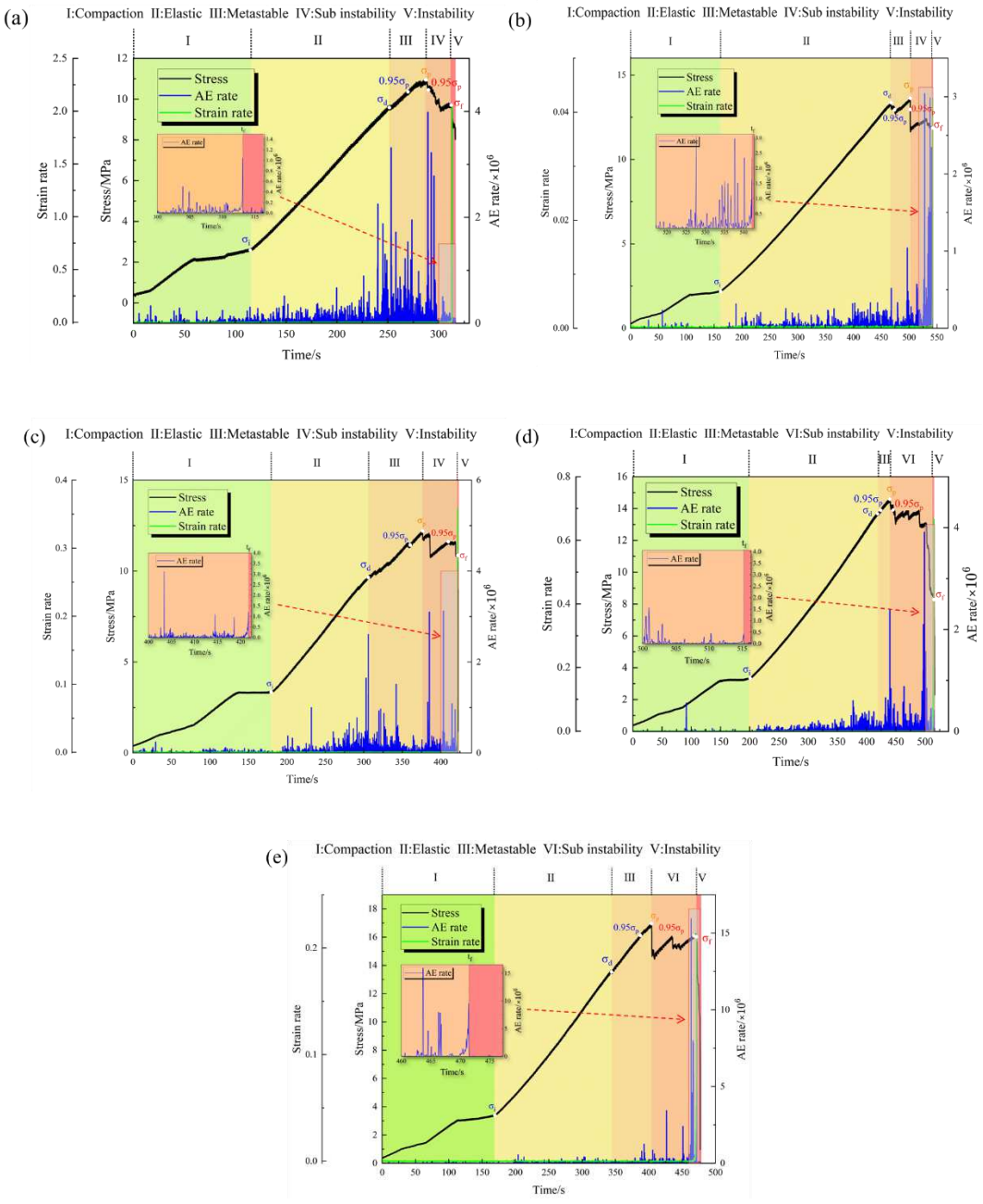


Figure 3. Temporal evolution curves of stress, strain rate, and AE rate for coal specimens with different opening shapes: (a) circular; (b) arched; (c) square; (d) trapezoidal; (e) complete

As shown in Figure 3, based on the coupled evolution of stress, strain rate, and AE rate, the entire loading process of the coal specimens is divided into five stages: compaction stage (I), elastic stage (II), metastable stage (III), sub-instability stage (IV), and instability stage (V). The characteristic stress points between stages include the crack initiation stress σ_i, crack damage stress σ_d, peak stress σ_p, and failure stress σ_f, with corresponding times t_i, t_d, t_p, and t_f, respectively.

As shown in Figure 3(a), the circular-opening coal specimen maintains low AE activity in stage (I), which gradually increases after entering stage (II), with bursts of AE activity occurring near t_d and t_p. In the early part of stage (IV), the AE activity declines, but both the AE rate and strain rate increase abruptly as t approaches t_f. From Figure 3(b), it can be seen that the AE rate of the arched-opening coal specimen exhibits relatively small fluctuations in stages (I) and (II). After entering stage (III), it surges abruptly near t_p, then drops back to nearly the same level as in stage (II). Near t_f, the AE rate shows multiple AE-rate peaks, while at the same time the strain rate, which had remained almost stable before, also increases sharply. As shown in Figure 3(c), the square-opening coal specimen has relatively concentrated AE activity near t_d, and both the AE rate and strain rate increase sharply near t_f. The AE rate of the trapezoidal-opening coal specimen surges near t_p, remains at a high level in stage (IV), and both the AE rate and strain rate increase sharply as t_f is approached, as detailed in Figure 3(d). For the complete coal specimen, the AE rate is relatively low throughout the entire loading process, with only a few high values appearing in stage (IV); within a short time before t_f, both the AE rate and strain rate show abrupt increases, as shown in Figure 3(e).

Although the five groups of coal specimens exhibit differences in AE evolution during the middle-early stages, their late-stage responses show consistency: AE activity intensifies in stage (IV), and both the strain rate and AE rate rise rapidly within a short time before t_f. This common feature provides an experimental basis for extracting acceleration-type indicators prior to catastrophic failure across different opening shapes.

As shown in Figure 2(b), the crack initiation stresses (σ_i) of coal specimens with different opening shapes are relatively close, ranging from 3.14 to 3.55 MPa, with an average value of 3.39 MPa. The percentage of σ_i relative to the peak stress (σ_p) of each coal specimen ranges from 22.16% to 33.9%. The variation trends of the damage stress (σ_d) and failure stress (σ_f) are in good agreement with the mean UCS of the five types of coal specimens.

The proportions of the durations of the metastable stage (III) and sub-instability stage (IV) relative to the total test time exhibit a certain correlation with the opening

shape. As shown in Figure 2(c), among the four types of opening-containing coal specimens, as the opening area decreases, the time proportion of the metastable stage (III) gradually increases from 9.05% for the circular-opening specimens to 16.66% for the trapezoidal-opening specimens; the proportion for the complete specimens is 11.54%, falling between those of the circular-opening and arched-opening specimens. As shown in Figure 2(d), the proportion of the sub-instability stage (IV) follows a slightly different pattern: the arched-opening specimens have the lowest proportion (3.49%), the trapezoidal-opening specimens have the highest (7.48%), and the complete specimens have a proportion of 7.15%, lying between the square-opening and trapezoidal-opening specimens.

3.3 Evolution characteristics of power-law singularity

3.3.1 Critical power-law acceleration characteristics of coal specimen failure

Figure 3 shows that coal specimens with five opening shapes all exhibit acceleration of the strain rate and AE rate near t_f. Previous studies have indicated that precursor signals such as cumulative AE events, cumulative rise time (Zhang and Zhou 2020), and the ratio of specimen deformation to the sum of displacements of the loading device and the specimen (Zhang et al. 2023) display similar characteristic acceleration trends prior to catastrophic failure, and such characteristic acceleration trends can be described by analogous scaling laws (Vasseur et al. 2015). To quantitatively describe the acceleration process of the response quantity Ω toward failure, the Voight empirical relationship (Voight 1988) is adopted:

$$\ddot{\Omega}\dot{\Omega}^{-\alpha} = A \tag{1}$$

where Ω is the observable response quantity, α is an exponent characterizing the degree of nonlinearity, and A is a constant.

The Voight relationship and its equivalent time-reversed power-law form have been applied in fields such as volcanic activity, earthquakes, and rock fracture instability time prediction (Zhang and Zhou 2020). Near system-level failure, the response quantity Ω can be expressed as (Xue et al. 2018; Vasseur et al. 2015):

$$\dot{\Omega}(t) = B_F(t_f - t)^{\beta_F} \tag{2}$$

where B_F is a constant, β_F is the critical power-law exponent, the subscript F denotes the failure time, and t_f is the time of system-level catastrophic failure.

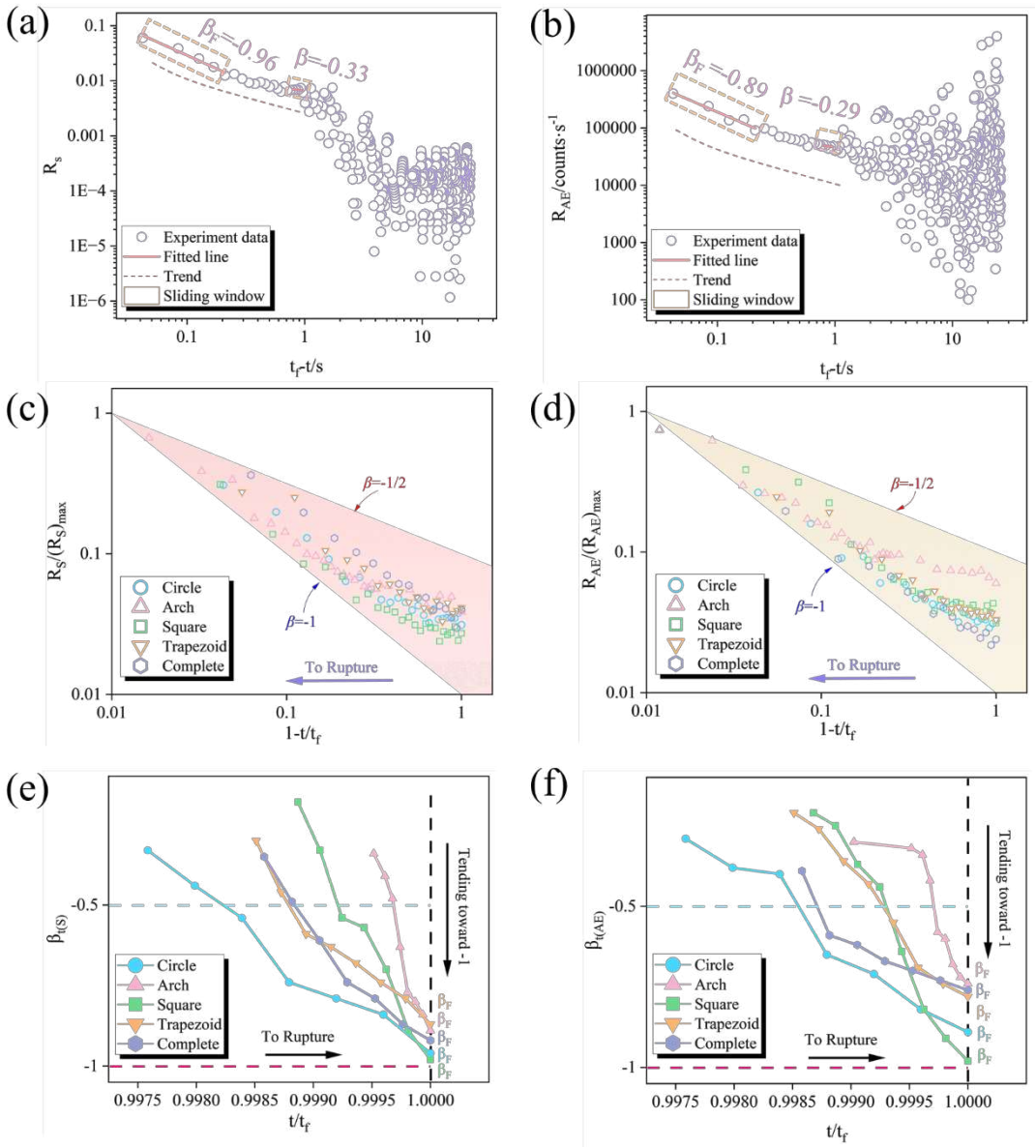


Figure 4. Power-law singularity of coal specimens with different opening shapes: (a)(b) power-law fitting curves of strain rate and AE rate for the circular-opening coal specimen; (c)(d) ranges of power-law exponents for strain rate and AE rate; (e)(f) evolution trends of power-law exponents for strain rate and AE rate approaching failure time

To verify whether the strain rate and AE rate before the time to failure (t_f) in the sub-instability stage (IV) satisfy Equation (2), the circular-opening representative specimen is taken as an example. The two types of response variables are plotted against the remaining time on double-logarithmic coordinates (Figure 4(a), (b)). The data

approximately within 1 s before failure exhibit a near-linear trend, indicating that both response variables possess power-law acceleration characteristics in the Sub instability stage. Moreover, the overall trend of the data is a slightly upward-concave curve, which can be confirmed by fitting the linear segments in Figure 4(a) and (b) using a sliding-window method with a fixed dataset size. It can be observed from the figures that the closer to the failure time, the smaller the slope of the window. Finally, taking the fitted slope of the linear segment of the imminent failure data as the critical power-law exponent β_F, the β_F values for the strain rate and AE rate of the circular-opening representative specimen are obtained as −0.96 and −0.89, respectively, with coefficients of determination R^2 of 0.97 and 0.96. The linear-segment data of the strain rate and AE rate near the failure time for representative specimens with different opening shapes are plotted in Figure 4(c) and (d). It is found that the data are generally distributed between the two reference lines of $\beta = -1$ and $\beta = -1/2$.

The sliding-window results further show that as failure approaches, the β values of most specimens gradually evolve from above −0.5 toward more negative critical values (Figure 4(e), (f)). A few specimens exceed the interval of −1 to −0.5, reflecting the influence of coal heterogeneity and intermittent local fracturing on instantaneous fitting. Therefore, a single representative specimen is not suitable for directly representing the ranking among groups; the opening geometric differences should be judged by combining the distribution and group mean of all valid specimens. The onset times of power-law singularity also differ among coal specimens with different opening shapes. In general, the circular-opening and trapezoidal-opening specimens exhibit earlier onset, the square-opening and arched-opening specimens show later onset, and the complete group falls in between.

3.3.2 Comparison of power-law acceleration behavior among different mechanical response variables

To compare the degree of late-stage acceleration between macroscopic deformation and internal microcracking activity within the same coal specimen, the ranges and group mean of β_F for the strain rate and AE rate were calculated respectively. The statistical results are listed in Table 1.

Table 1 Statistical results of β_F for mechanical response variables of coal specimens with different opening shapes

		Circle	Arch	Square	Trapezoid	Complete
Range of values	Strain rate	-1.12~-0.29	-1.33~-0.44	-1.35~-0.61	-1.15~-0.77	-1.19~-0.57
	AE rate	-1.33~-0.33	-0.91~-0.35	-1.22~-0.49	-1.18~-0.5	-1.21~-0.47
Group mean	Strain rate	-0.72	-0.93	-0.95	-0.98	-0.92
	AE rate	-0.83	-0.65	-0.75	-0.79	-0.74

Table 1 shows that for the same coal specimen, the β_F values derived from the strain rate and AE rate are mostly in the range of −1 to −0.5, indicating that both surface macroscopic deformation and internal microcracking activity share the fundamental scaling of power-law acceleration in the Sub instability stage. Except for the circular-opening coal specimens, the range of β_F for the AE rate is higher than that for the strain rate in the remaining coal specimens. Specifically, for the circular-opening coal specimens, the strain rate β_F is greater than the AE rate β_F, and the minimum values of both are below −1. For the arched-opening coal specimens, the AE rate β_F values are entirely at relatively high levels, all greater than −1, with a relatively small fluctuation range of only 0.56; whereas the strain rate exhibits a much larger fluctuation range of 0.89, indicating that the generation and propagation of internal micro-damage before catastrophic failure in arched-opening coal specimens are more stable than the process of macroscopic crack formation and coalescence that leads to a sudden surge in strain rate. For the square-opening coal specimens, the variation ranges of β_F for the AE rate and strain rate are almost identical, with the strain rate at 0.74 and the AE rate at 0.73. For the trapezoidal-opening and complete coal specimens, the variation ranges of the AE rate β_F are also generally larger than those of the strain rate.

Overall, except for the circular-opening coal specimens, the strain rate β_F is

relatively lower than the AE rate β_F for the remaining coal specimens, making it a more pronounced precursor feature of coal specimen failure. For the circular-opening specimens, the opposite is true, with the critical power-law acceleration of the AE rate being more prominent. The AE rate is more sensitive to the rapid activation of local microcrack clusters, whereas the strain rate depends on whether crack propagation has already formed a distinguishable localization band on the observed surface. The two response variables share a common imminent failure acceleration mechanism but cannot substitute for each other.

3.3.3 Influence of opening shape on power-law acceleration behavior of response variables

To investigate the inter-group differences of the same response quantity under different opening shapes, the β_F data of all valid specimens in each group are plotted as boxplots, with the group means connected by spline curves (Figure 5).

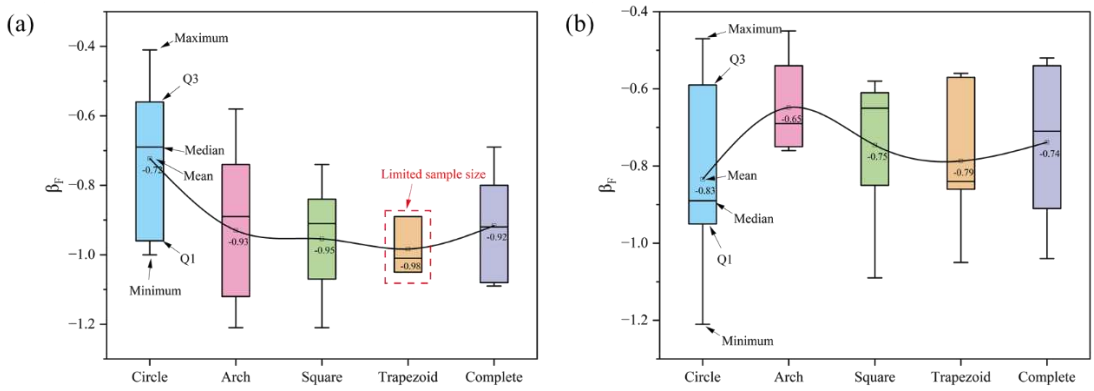


Figure 5. Statistical characteristics of β_F for coal specimens with different opening shapes: (a) strain rate; (b) AE rate

In Figure 5(a), the mean β_F values of the strain rate are −0.72 for the circular-opening group, −0.93 for the arched-opening group, −0.95 for the square-opening group, −0.98 for the trapezoidal-opening group, and −0.92 for the complete coal specimens. It can be seen that the macroscopic deformation acceleration is strongest in the trapezoidal-opening and square-opening coal specimens, was similar for the arched-opening and complete groups, and weakest in the circular-opening specimens. The box of the trapezoidal-opening specimens is the narrowest, indicating relatively high intra-group consistency of the strain rate β_F; the arched-opening,

square-opening, and complete specimens exhibit larger scatter, suggesting that the localization path is more significantly influenced by pre-existing defects.

Figure 5(b) gives the mean β_F values of the AE rate as −0.83, −0.65, −0.75, −0.79, and −0.74, respectively, which do not follow the same ranking as the strain rate. The AE acceleration is strongest in the circular-opening coal specimens, followed by the trapezoidal-opening specimens, and weakest in the arched-opening specimens. The circular-opening specimens also exhibit a relatively wide range of exponent values, indicating that the symmetric stress field around the opening may promote concentrated intensification of microcracking activity, but the locations of such activity are not always synchronized with surface strain localization. The difference in ranking between the two response variables further demonstrates that the opening opening geometry regulates microcracking activity and macroscopic deformation in different ways; joint monitoring covers a broader range of failure modes than a single indicator.

3.4 Critical slowing-down phenomenon prior to catastrophic failure

When a dynamical system approaches a critical transition, fluctuation amplitude and persistence increase, while recovery becomes slower and weaker. This phenomenon is termed the critical slowing-down phenomenon (Zhu et al. 2022). Previous studies have shown that critical slowing-down also exists during rock loading-induced failure tests, and the two statistical parameters, namely the variance and autocorrelation coefficient of the system's AE characteristic parameters, often exhibit an increasing trend (Zhang et al. 2025b; Lei et al. 2025). In this paper, the variance and autocorrelation coefficient are adopted to characterize the critical slowing-down features of the strain rate and AE rate. The analysis procedure is shown in Figure 6.

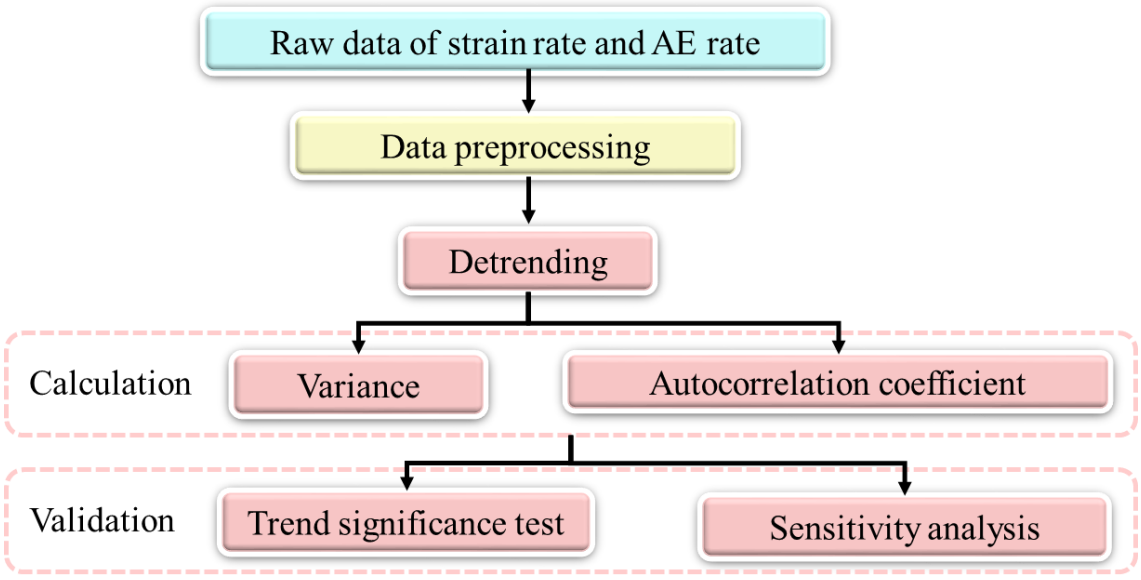


Figure 6. Flowchart of critical slowing-down analysis

3.4.1 Critical slowing-down phenomenon of response variables

(1) Gaussian-kernel detrending

The original response-rate sequence usually contains both a long-term evolutionary trend and short-term fluctuations. To prevent the long-term trend from inflating the variance and autocorrelation coefficient, a Gaussian-kernel smoothing method is used to estimate the trend before calculating the critical slowing-down indicators, and the difference between the original sequence and the trend term is taken as the residual sequence.

$$\hat{x}_i = \sum_{j=1}^{N} x_j \cdot \frac{\exp(-\frac{(i-j)^2}{2d^2})}{\sum_{k=1}^{N} \exp(-\frac{(i-k)^2}{2d^2})} \tag{3}$$

$$r_i = x_i - \hat{x}_i \tag{4}$$

where x_i is the original data at the i-th time point, N is the length of the time series, d is the standard deviation of the Gaussian kernel that controls the smoothing scale (taken as 10%–20% of the sequence length in this study), $\hat{x}_i$ is the estimated trend value at the i-th point, and r_i is the residual after detrending. Both metrics were subsequently calculated from r_i.

(2) Variance and autocorrelation coefficient

The variance describes the degree of deviation of the data in a specimen from the mean value. When the system approaches a critical transition, its recovery capability

deteriorates, and accordingly, the variance increases. The variance is calculated as:

$$S^2 = \frac{1}{n}\sum_i^n (x_i - \bar{x})^2 \tag{5}$$

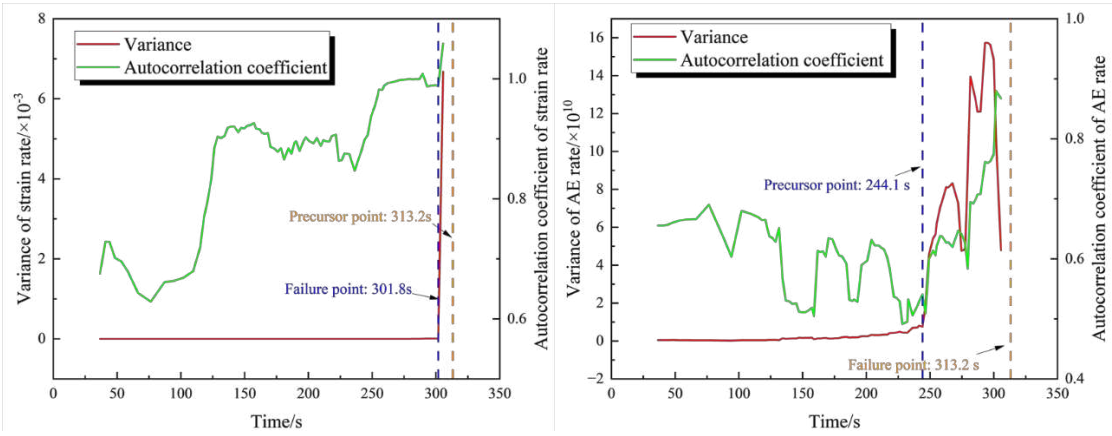
Where S^2 is the variance, x_i is the i-th data point, $\bar{x}$ is the mean value, and n is the number of data points in the sequence.

The autocorrelation coefficient measures the persistence of the same variable at different times. When the system recovery rate decreases, the memory between adjacent states strengthens, and the autocorrelation coefficient generally increases. It is calculated as:

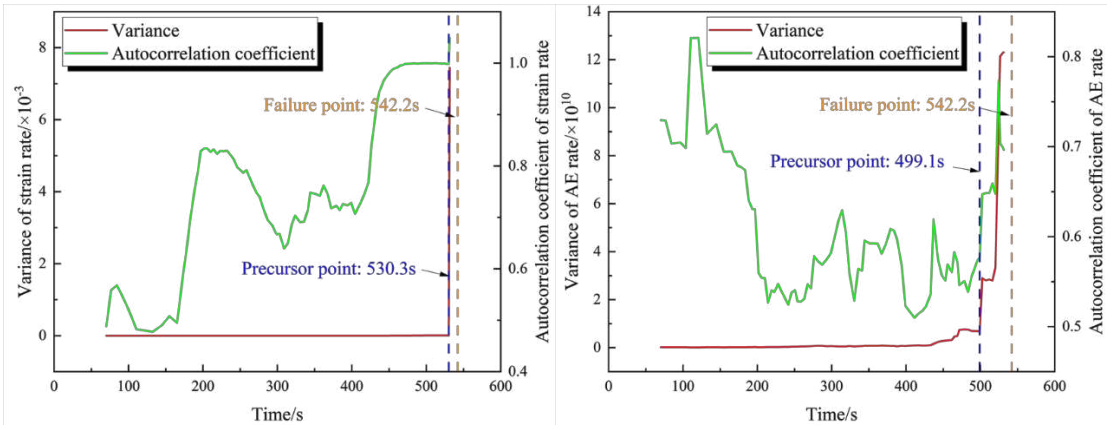
$$a(j) = \sum_{i=1}^{n-j} \left(\frac{x_i - \bar{x}}{S}\right)\left(\frac{x_{i+j} - \bar{x}}{S}\right) \tag{6}$$

where S is the standard deviation, j is the lag length, x_i is the i-th data point, x_{i+j} is the (i+j)-th data point, $\bar{x}$ is the mean value, and n is the number of data points in the sequence.

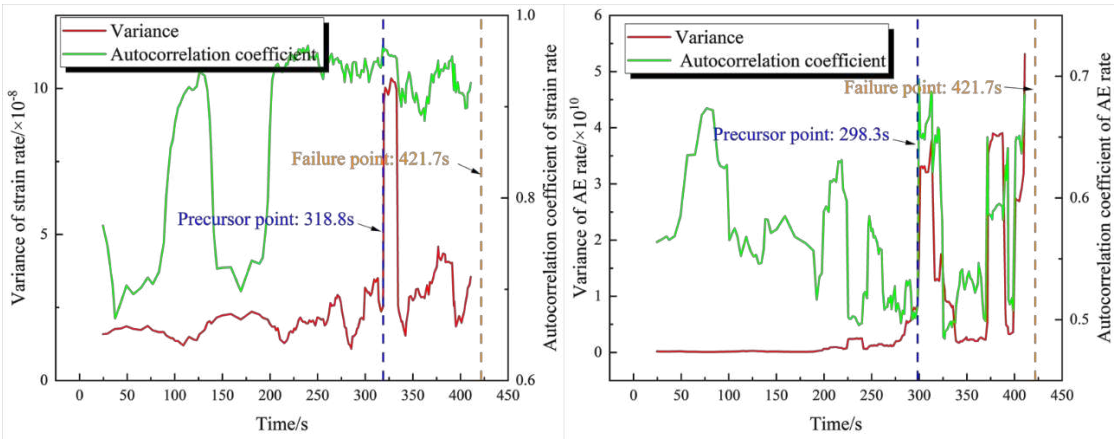
The calculation of the variance and autocorrelation coefficient requires determining the time window length and the lag step. Zhu Xing et al. [1] found that the time window length and lag step have negligible influence on the precursor information and can be disregarded. Therefore, in this study, considering the sequence length of each specimen, the baseline calculation adopts a time window length of 1000 and a lag step of 100. The robustness of the results is verified in Section 3.4.4 through multi-parameter combination tests. The evolution of the variance and autocorrelation coefficient of the strain rate and AE rate for representative specimens is shown in Figure 7.



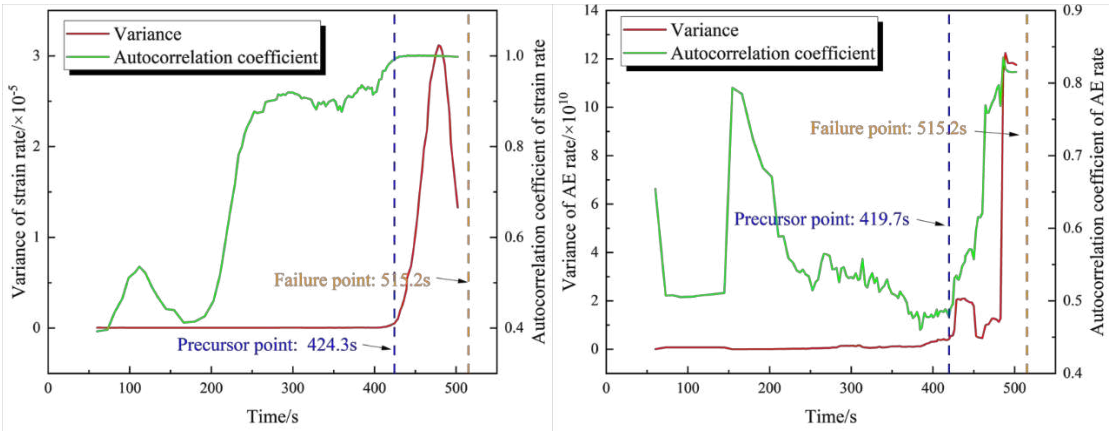
（a）Circle



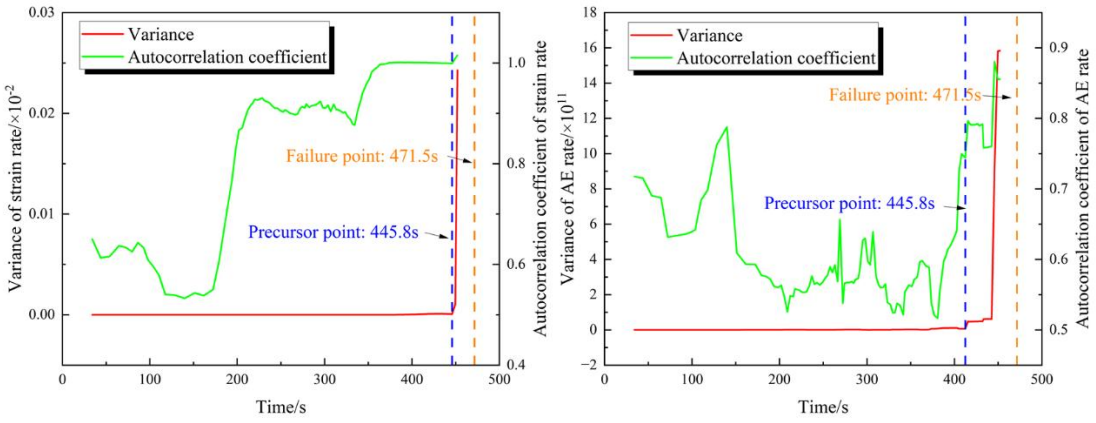
（b）Arch



（c）Square



（d）Trapezoid



（e）Complete

Figure 7. Evolution curves of critical slowing-down indicators for strain rate and AE rate of typical coal specimens with different opening shapes

Figure 7 shows that for the five types of coal specimens with different opening shapes, critical slowing-down signals, such as increasing variance or enhancing autocorrelation, appear in both the strain rate and AE rate as failure approaches. The autocorrelation coefficient curves are noticeably more fluctuating and less stable than the variance curves, which is consistent with the findings of (Zhu et al. 2022) and (Zhang et al. 2025b) on other rock types. The variance remains relatively stable in the early stage and increases abruptly in the Sub instability stage. Therefore, in this paper, the moment when the variance suddenly increases is taken as the precursor point of coal specimen failure, with changes in the autocorrelation coefficient serving as auxiliary evidence. The failure point has been determined from the experimental results.

There are systematic differences in the precursor times given by the two response variables. The precursor points derived from the AE rate consistently occur earlier than those from the strain rate. Specifically, for the circular-opening coal specimens, the strain-rate and AE-rate precursor points precede the failure point by approximately 11.4 s and 69.1 s, respectively, with a difference of 57.7 s—the largest difference between the strain-rate and AE-rate precursor times among the five types of specimens. For the arched-opening specimens, the precursor points precede failure by about 11.9 s and 43.1 s, respectively, with a difference of over 30 s. For the square-opening specimens, both precursors appear more than 100 s in advance, with the AE-rate precursor occurring

123.4 s ahead, meaning that the critical slowing-down phenomenon appears at about 70% of the total loading time. For the trapezoidal-opening specimens, the precursor points precede failure by approximately 90.9 s and 95.5 s, respectively, with a difference of only 4.6 s. For the complete specimens, both precursors appear at 445.8 s, preceding the failure point by about 25.7 s.

Overall, the AE-rate precursor occurs no later than the strain-rate precursor, indicating that microcracking activity generally enters an anomalous fluctuation state before observable macroscopic deformation does. However, the lead times for the square-opening and trapezoidal-opening specimens are considerably larger, suggesting that early precursors may contain information on local damage adjustment rather than immediate instability. Therefore, critical slowing-down is better suited for early risk screening rather than for precise prediction of failure time when used alone.

3.4.2 Comparison of precursor timing and stress level of critical slowing-down

To compare the similarities and differences in the critical slowing-down precursor characteristics among coal specimens with different opening shapes, from a temporal perspective, the ratio of the precursor occurrence time to the failure time is defined as the critical time coefficient of coal specimen failure, denoted as α_c. In this study, α_c includes the critical time coefficient derived from the strain rate, α_{cs}, and that derived from the AE rate, α_{ca}. Figure 8 shows that the α_{cs} of the square-opening coal specimens is as high as 0.91, indicating that the precursor appears very late, close to the failure time, whereas the αcs of the complete specimens is relatively lower at only 0.85, suggesting that the strain rate can respond to the impending failure of complete specimens with a considerably longer lead time. Moreover, the α_{cs} and α_{ca} of the complete specimens are very close to each other, indicating that the strain rate and AE rate of the complete specimens respond almost simultaneously.

The mean α_{cs} values of the five types of coal specimens range from 0.85 to 0.91, while the mean α_{ca} values range from 0.78 to 0.84. The α_{cs} values are closer to 1, indicating that the AE rate is more sensitive to early microcrack reorganization, whereas the strain rate generally exhibits stable precursors only after further localization of damage; that is, the strain rate can predict the failure time of coal specimens more

accurately than the AE rate. Therefore, the subsequent analyses are based on the precursor time obtained from the variance of the strain rate.

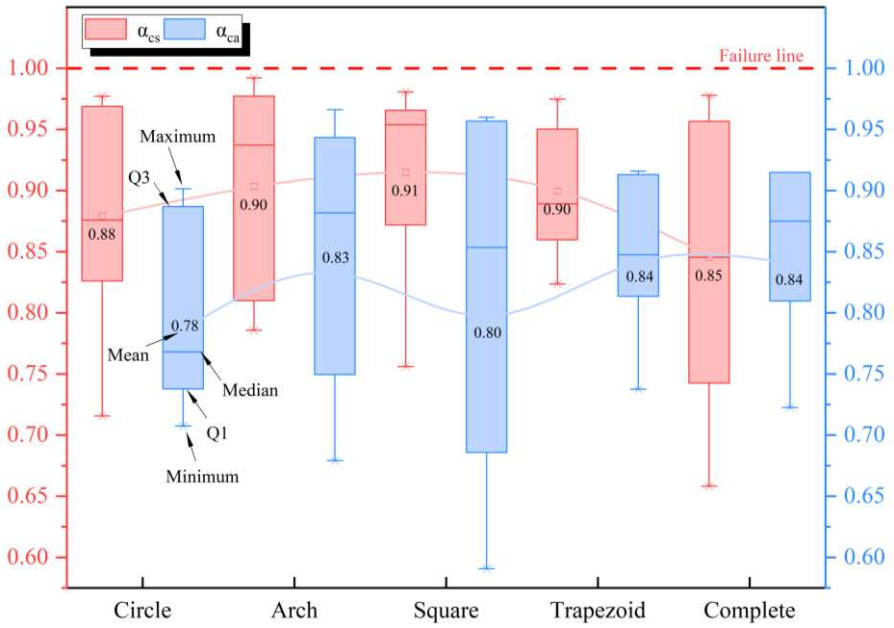


Figure 8. α_{cs} and α_{ca} of coal specimens with different opening shapes

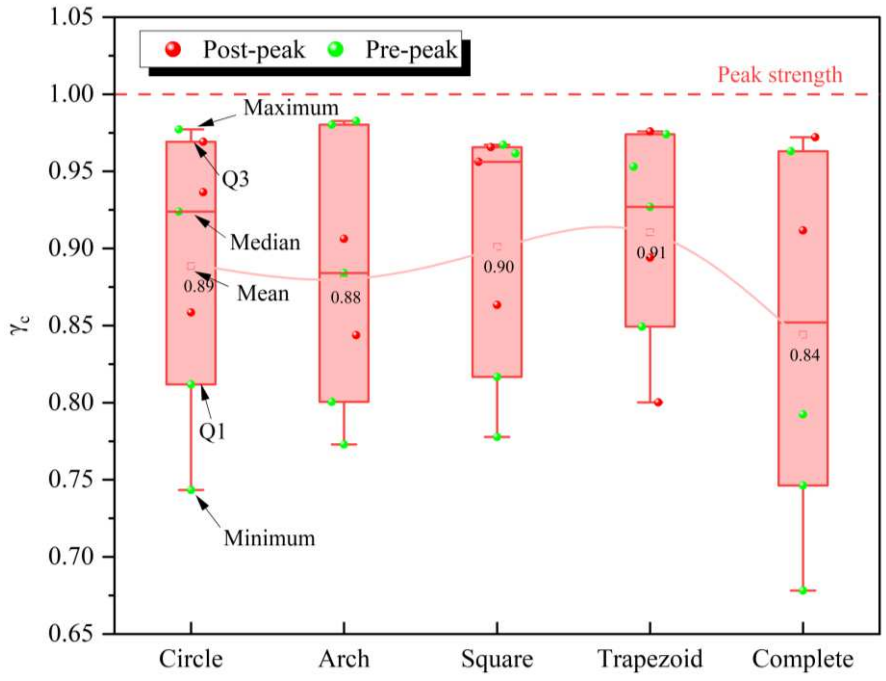


Figure 9 γ_c of strain rate for coal specimens with different opening shapes

From the perspective of strength, the ratio of the precursor stress to the peak stress is defined as the critical strength coefficient of coal specimen failure, denoted as γ_c. In Figure 9, the mean γ_c values for the five types of coal specimens with different opening shapes are 0.89, 0.88, 0.90, 0.91, and 0.84, respectively. Except for the complete group,

the group mean of the opening-containing specimens are concentrated between 0.88 and 0.91, indicating that the critical slowing-down precursors generally occur in the damage acceleration stage near the peak stress. The complete specimens exhibit the lowest group mean and the widest distribution, suggesting that the transition of localized damage, dominated by pre-existing defects, shows stronger individual variability. Furthermore, in about 62% of all specimens, the precursor point occurs before the peak stress, meaning that the majority of coal specimens exhibit precursor characteristics before reaching the peak stress.

3.4.3 Analysis of significance test results

To test whether the critical slowing-down phenomena of the strain rate and AE rate obtained above are significant, the Mann–Kendall trend test is performed on the four indicators: strain-rate variance, strain-rate autocorrelation coefficient, AE-rate variance, and AE-rate autocorrelation coefficient. The calculation procedure is as follows:

(1) Construct the statistic S:

$$S = \sum_{p=1}^{n-1} \sum_{q=p+1}^{n} sgn(y_q - y_p) \tag{7}$$

where y is the critical slowing-down indicator sequence, and n is the length of the indicator sequence.

(2) The sign function is defined as:

$$sgn(y_q - y_p) = \begin{cases} +1 & if\, y_q > y_p \\ 0 & if\, y_q = y_p \\ -1 & if\, y_q < y_p \end{cases} \tag{8}$$

(3) Calculate Kendall's Tau correlation coefficient:

$$\tau = \frac{S}{D} \tag{9}$$

where D is the total number of data pairs, used to normalize S to the interval [−1,1].Under the standard definition, $D = \frac{n(n-1)}{2}$. The Kendall's Tau (τ) ranges from [−1,1], with a positive value indicating a monotonic increase of the indicator over time and a negative value indicating a monotonic decrease.

(4) Basis for calculating the P-value (significance probability)

When n is sufficiently large, S approximately follows a normal distribution, and its variance is given by:

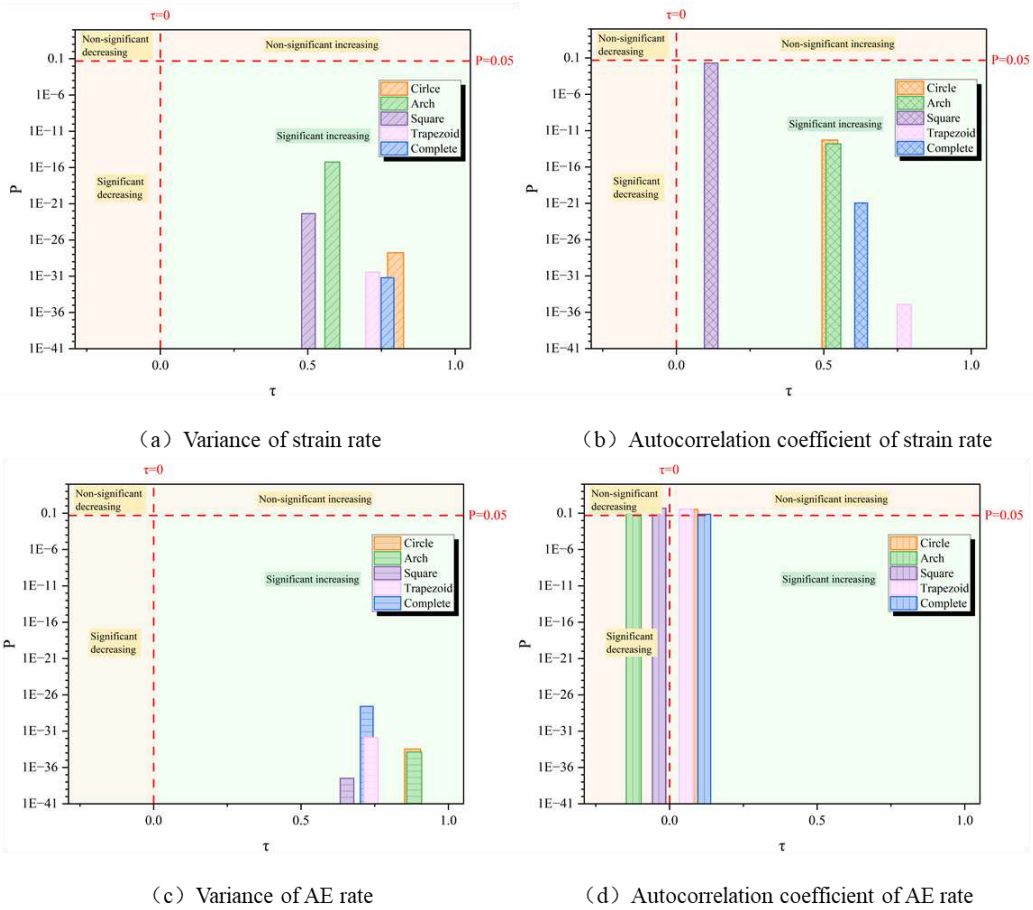
$$Var(S) = \frac{n(n-1)(2n+5)}{18} \tag{10}$$

The standardized score Z is calculated as: $Z = \frac{S}{\sqrt{Var(S)}}$,the P-value is obtained by consulting the standard normal distribution table based on Z. The P-value represents the probability of erroneously rejecting the null hypothesis (no trend). When $P<0.05$ (i.e., at the 5% significance level), the null hypothesis of "no trend" is rejected. In this paper, a trend with $\tau>0$ and $P<0.05$ is judged as a significant increasing trend.

The test results for the representative specimens are shown in Figure 10. Based on the sign of τ and whether P is less than 0.05, the results can be classified into four regions: significant increasing, significant decreasing, non-significant increasing, and non-significant decreasing. For all representative specimens, the autocorrelation coefficient of the AE rate falls into the non-significant region, while the remaining indicators all lie in the significant increasing region. This result indicates that the critical slowing-down trend of the strain-rate sequence is generally stronger than that of the AE-rate sequence; among the two statistical indicators, the increasing trend of the variance is more stable than that of the autocorrelation coefficient, and thus is more suitable as the primary criterion.

Figure 11 summarizes the trend significance test results for all specimens. The number of indicators passing the significance test among the four indicators is defined as the comprehensive significance level: when 4, 3, 2, and 1 indicator(s) are significant, the levels are designated as "significant", "relatively significant", "moderate", and "relatively non-significant", respectively. The overall levels of the complete, arched-opening, and circular-opening coal specimens are relatively high, while those of the square-opening and trapezoidal-opening specimens are relatively low; in particular, the trapezoidal-opening specimens have at least one indicator that does not reach the significance level. The multi-source crack propagation induced by angular openings may enhance intermittent fluctuations in the response sequences, thereby weakening the monotonic trend; this interpretation still needs to be verified with crack

localization or fracture surface evidence.



（a）Variance of strain rate　（b）Autocorrelation coefficient of strain rate

（c）Variance of AE rate　（d）Autocorrelation coefficient of AE rate

Figure 10. Trend significance test results for typical coal specimens with different opening shapes

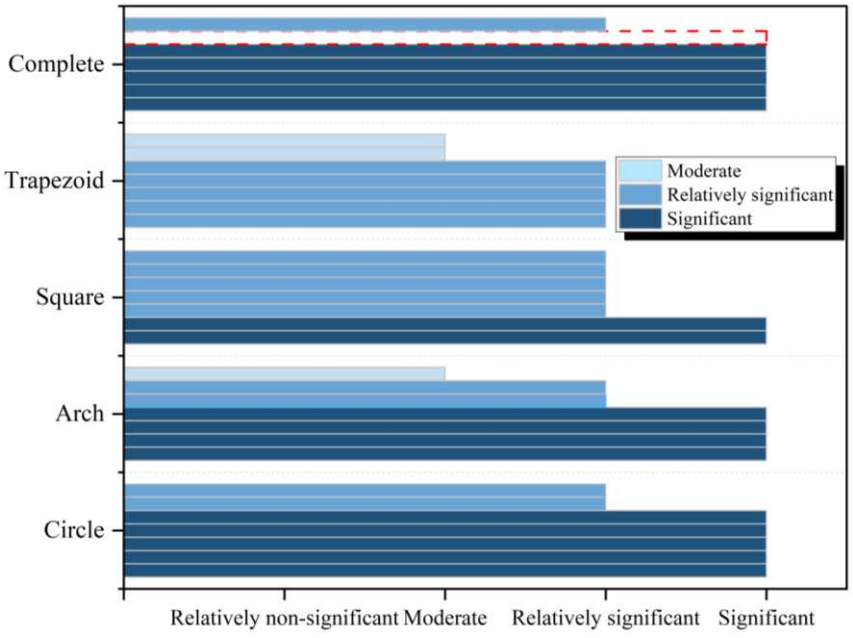


Figure 11. Trend significance test results for all coal specimens

3.4.4 Analysis of robustness test results

To determine whether the critical slowing-down signals are artificially generated by specific parameter combinations, the Gaussian kernel bandwidth d and the sliding window length W were varied, and τ was recalculated accordingly.

$$\tau(d, W) \; for \; \forall d \in D_{grid}, \forall W \in W_{grid} \tag{11}$$

where D_{grid} is the candidate set of detrending bandwidths: {0.08, 0.12, 0.16, 0.20}, and W_{grid} is the candidate set of sliding-window relative lengths: {0.3, 0.4, 0.5, 0.6, 0.7}.

The ranges of τ for the strain rate of coal specimens with different opening shapes are listed in Table 2. Overall, the τ range of the variance is not lower than that of the autocorrelation coefficient, indicating that the increasing trend of the variance is more robust to parameter selection. Taking the circular-opening typical coal specimen as an example, Figure 12 shows the τ heatmaps under the 20 d-W combinations; the dark regions corresponding to higher τ values are more continuous and cover a larger area in the variance maps. Similar conclusions are obtained for the remaining coal specimens. Therefore, within the current data and parameter ranges, the variance can serve as the primary indicator of critical slowing-down, while the autocorrelation coefficient is better suited as an auxiliary verification indicator.

Table 2. Robustness test results of strain rate for coal specimens with different opening shapes

Cross-sectional shape	Range of τ values	
	Variance	Autocorrelation coefficient
Circle	0.50~1	0.05~0.99
Arch	0.04~1	0.02~1
Square	0.52~1	0.25~1
Trapezoid	-0.69~1	-0.82~0.91
Complete	-0.56~1	-0.62~0.98

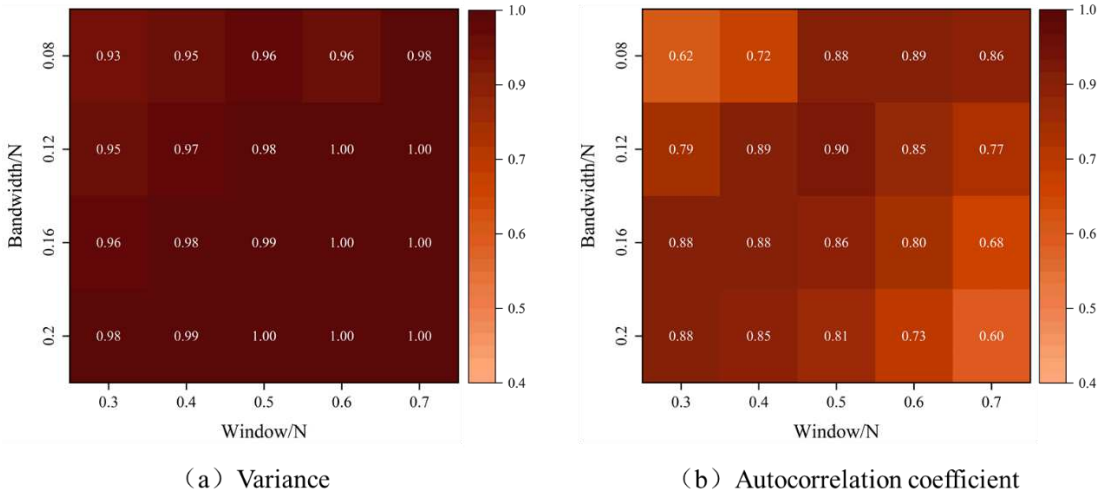


Figure 12. Sensitivity analysis heatmaps of variance and autocorrelation coefficient of strain rate for a representative circular-opening coal specimen

4 Discussion

4.1 Correlation analysis between power-law singularity and critical slowing-down

4.1.1 Unified physical basis of the two precursor phenomena

Figure 8 shows that the critical slowing-down precursors appear on average at 78%–91% of the time to t_f. Referring to Table 3, this mainly corresponds to the late elastic stage (II) to the metastable stage (III), i.e., the interval in which coal damage transitions from near-linear accumulation to nonlinear evolution. Power-law acceleration is concentrated approximately 1 s before failure, mainly corresponding to the sub-instability stage (IV), during which the AE rate of the coal specimens is high and multiple maximum values appear. This may be related to the development of internal microcracks and their coalescence into macroscopic cracks. In summary, the emergence of the two types of precursors reflects different degrees of internal damage evolution in the coal specimens. The critical slowing-down phenomenon of both the strain rate and AE rate occurs during the transition of internal damage from steady to accelerating development, appearing earlier than the power-law acceleration phenomenon. During the process of accelerated damage propagation, these scattered micro-damages within the coal specimen converge and connect to form macroscopic fracture zones, at which point the strain rate and AE rate response variables exhibit power-law acceleration. The two types of precursors are driven by the same damage

evolution process but correspond to different timescales: critical slowing-down reveals the degradation of system recovery capability, providing a longer lead time; power-law acceleration characterizes the divergence of the response rate near failure, offering higher temporal localization accuracy.

Table 3. Ratios of characteristic stress times to failure time for coal specimens with different opening shapes

Cross-sectional shape	t_i/t_f	t_d/t_f	t_p/t_f	t_f/t_f
Circle	0.525	0.865	0.956	1
Arch	0.416	0.831	0.965	1
Square	0.454	0.794	0.943	1
Trapezoid	0.391	0.758	0.925	1
Complete	0.389	0.809	0.928	1

4.1.2 Synergistic/complementary relationship between the two precursors

Based on the comprehensive significance levels of each group summarized in Figure 11, the clarity of critical slowing-down for coal specimens with different opening shapes, ranked from low to high, is: trapezoid < square < complete < arch < circle. Table 4 presents the mean critical power-law exponents of the strain rate and AE rate for coal specimens with different opening shapes; smaller values indicate stronger imminent failure acceleration. The combined group mean, ranked from weak to strong, are: circle < arch < complete < square < trapezoid. The two rankings are approximately opposite: the square-opening and trapezoid-opening specimens, which exhibit weaker critical slowing-down, show stronger late-stage power-law acceleration, while the circular-opening and arched-opening specimens, which exhibit clearer critical slowing-down, show relatively weaker late-stage acceleration. This complementary relationship indicates that a single indicator may have a sensitivity bias toward specific opening geometries, and the combined use of both can reduce the risk of missed alarms. The two types of critical precursors thus exhibit a complementary relationship.

Table 4. Mean critical power-law exponents of strain rate and AE rate for coal specimens with different opening shapes

	Circle	Arch	Square	Trapezoid	Complete
Mean	-0.78	-0.79	-0.85	-0.89	-0.83

4.2 Prediction method based on the two precursor characteristics

Based on the above results, a dual-timescale early warning framework consisting of "early risk identification—final-stage imminent failure confirmation" is constructed (Figure 13). In the early loading stage, the synchronous strain-rate and AE-rate sequences are detrended, and the variance and autocorrelation coefficient are calculated within a sliding window. When the variance shows a sustained and significant increase, and passes the Mann–Kendall test and parameter sensitivity test, an early attention signal is issued; the AE rate is used to enhance early sensitivity to microcracking activity, while the strain rate is used to confirm the macroscopic deformation response. In the later loading stage, the double-logarithmic fitting of the response rate versus the remaining time is continuously updated. If the strain rate or AE rate exhibits a stable power-law regime with consistently high goodness-of-fit, and β continues to evolve toward the calibrated critical range, the alert is escalated to an imminent-failure warning. The two-stage evidence is linked in chronological order, balancing the advance warning time and the accuracy of failure time identification.

The thresholds in this framework should be calibrated according to the monitoring object and noise level. In this experimental study, β_F is mainly distributed in the range of −1 to −0.5; therefore, in engineering applications, it is not advisable to mechanically adopt a single β threshold. A more robust criterion is to simultaneously examine the continuous decrease of β, the stability of the linear regime, the goodness-of-fit, and the consistency between the strain rate and AE rate. If only critical slowing-down appears without stable power-law acceleration, the monitoring should be maintained with continued attention; if both types of evidence appear sequentially, the warning level should be raised to the imminent-failure state. This method still requires prospective validation under different stress paths, scales, and field noise conditions.

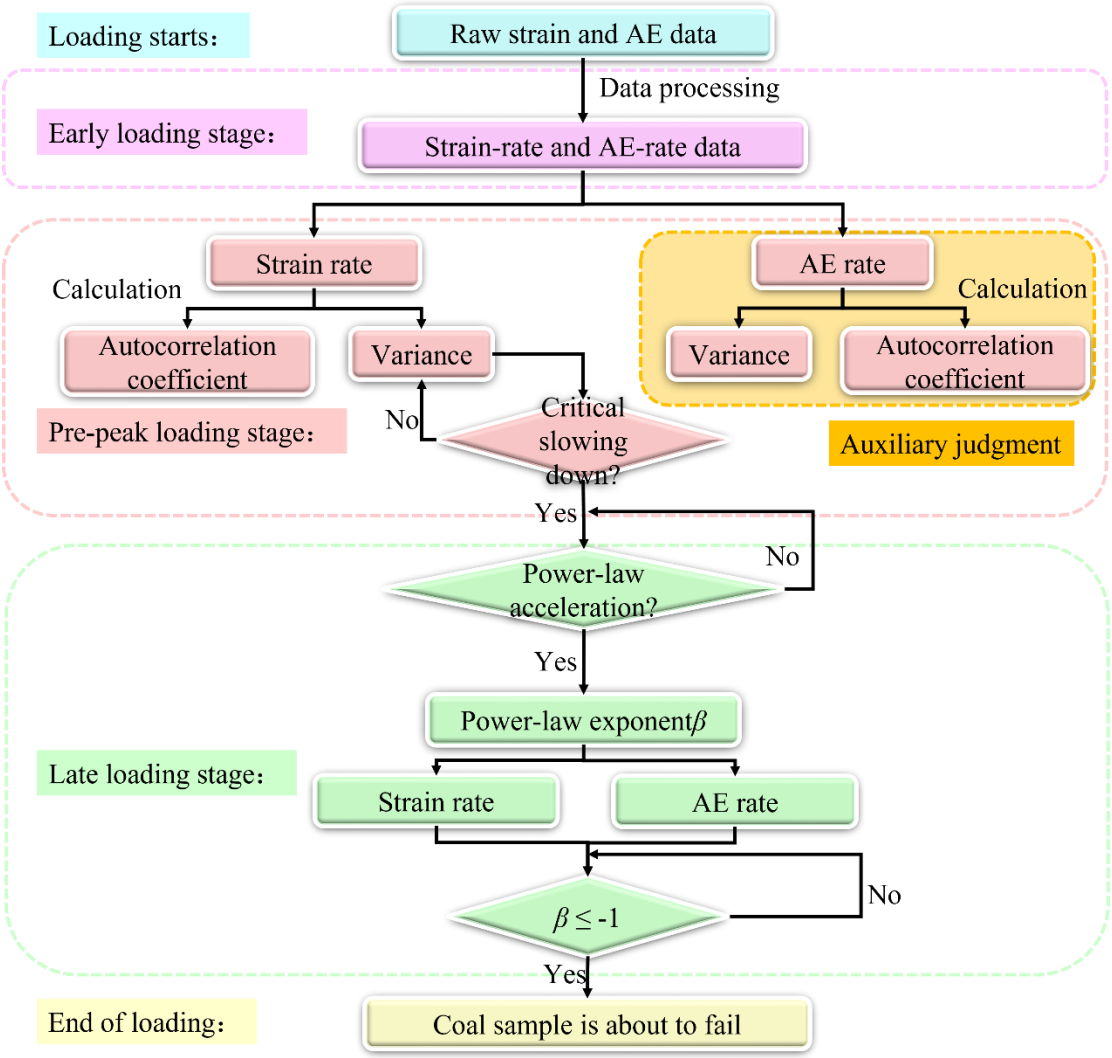


Figure 13. Schematic flowchart of the dual-timescale prediction strategy

5 Conclusions

Through laboratory experiments, this paper investigates the critical power-law singularity and critical slowing-down phenomena of two response variables—strain rate and AE rate—prior to catastrophic failure of deep roadway surrounding rock under realistic stress conditions, and analyzes the similarities and differences in the evolution characteristics of coal specimens with different opening shapes. The main conclusions are as follows:

(1) The opening opening geometry significantly alters the load-bearing capacity and damage stages of the coal specimens. The mean UCS of the five groups, from lowest to highest, follows the order: circular opening, square opening, trapezoidal opening, arched opening, and complete specimen. The circular-opening specimens

have the lowest strength deterioration coefficient of 0.73, while the arched-opening specimens have the highest of 0.98. The σ_i values of all groups are relatively close, whereas the differences in σ_d, σ_f, and the durations of stages III–IV are more pronounced, indicating that the opening geometry mainly affects the crack propagation and coalescence process. Since the opening areas differ among the shapes, the above trends should be interpreted as a combined shape-area effect.

(2) Both the strain rate and AE rate exhibit power-law acceleration prior to t_f, but their sensitivities to opening geometry differ. The group-mean β_F for the strain rate ranges from −0.72 to −0.98, with the strongest acceleration observed in the trapezoidal-opening and square-opening specimens. The group-mean β_F for the AE rate ranges from −0.65 to −0.83, with the circular-opening specimens showing the strongest acceleration. The two indicators share the imminent failure acceleration scaling, but their inter-group rankings and single-specimen synchrony differ, reflecting a spatiotemporal mismatch between microcracking activity and macroscopic strain localization.

(3) Critical slowing-down appears in all five types of coal specimens. The mean α_c for the strain-rate precursors ranges from 0.85 to 0.91, and that for the AE-rate precursors ranges from 0.78 to 0.84, with the latter generally occurring earlier. The mean γ_c of the precursor points ranges from 0.84 to 0.91, mostly located near the peak stress. The Mann–Kendall test and parameter sensitivity analysis indicate that the increasing trend of the variance is more significant and more robust than that of the autocorrelation coefficient, making it suitable as the primary criterion; the autocorrelation coefficient can serve as auxiliary verification.

(4) Critical slowing-down and power-law acceleration correspond to different damage scales. The former identifies the degradation of system recovery capability and can provide a longer risk window; the latter characterizes the divergence of the response rate near failure and can improve the accuracy of failure time identification. On this basis, a dual-timescale prediction strategy is proposed, in which a sustained significant increase in variance triggers early attention, and a stable power-law regime with β continuously evolving toward the critical range triggers imminent-failure confirmation.

This method is supported by consistent evidence from the present laboratory experiments, but its threshold transferability still needs to be validated through equal-area opening-shape tests, complex stress paths, and prospective field data.

CRediT authorship contribution statement

Ji Ma: Formal analysis, Methodology, Data curation, Conceptualization, Writing – review & editing, Funding acquisition. **Zhouyang Jiang**: Writing – original draft, Investigation, Visualization. **Housheng Jia**: Supervision, Resources. **Ruifu Yuan**: Supervision, Formal analysis. **Zhiqiang Hou**: Formal analysis, Project administration. **Lifang Feng:** Investigation, Visualization, Software**. Zhengxuan Yang:** Visualization, Investigation. **Xiao Li**: Investigation, Visualization.

Declaration of competing interest

The authors declare that they have no known competing financial interests or personal relationships that could have appeared to influence the work reported in this paper.

Acknowledgments

This study is funded by the National Natural Science Foundation of China (52404119), Open Fund of the State Key Laboratory of Coalburst Theory and Prevention Technology National Mine Safety Administration(Preparatory) (Grant No. KFJJ-2025-0018) and the Zhongye Changtian Scientific Research and Development Basic Research Foundation (Grant No. 2026JCYJ13).

References

[1] Cheng L, Hao S, Lu C (2024a) Precursory deformation responses in different directions to catastrophic failure of uniaxially compressed sandstones. Arch Mech 76(1-2):39-60. https://doi.org/10.24423/aom.4378

[2] Cheng L, Hao S, Lu C (2024b) Spatial heterogeneity of precursory accelerating deformation in uniaxially compressed sandstones and prediction of failure time. J Build Eng 82:108201. https://doi.org/10.1016/j.jobe.2023.108201

[3] Cheng L, Hao S, Lu C, Zhou S (2024c) Two typical phases of failure acceleration in rocks under uniaxial compression. Heliyon 10(1):e24003. https://doi.org/10.1016/j.heliyon.2024.e24003

[4] Dai L, Pan Y, Li Z, Wang A, Xiao Y, Liu F, Shi T, Zheng W (2021) Quantitative mechanism of roadway rockbursts in deep extra-thick coal seams: theory and case

histories. Tunn Undergr Space Technol 111:103861. https://doi.org/10.1016/j.tust.2021.103861

[5] Fan C, Liu J, Meng F (2024) Microcracking process characterization and failure time prediction of three typical rocks upon uniaxial compression based on acoustic emission activity. Rock Mech Rock Eng 57(11):9145-9164. https://doi.org/10.1007/s00603-024-04093-0

[6] Fan L, Wang W, Yuan C, Peng W (2020) Research on large deformation mechanism of deep roadway with dynamic pressure. Energy Sci Eng 8(9):3348-3364. https://doi.org/10.1002/ese3.672

[7] Hao SW, Rong F, Ming-Fu L, Wang HY, Xia MF, Fu-Jiu K, Bai YL (2013) Power-law singularity as a possible catastrophe warning observed in rock experiments. Int J Rock Mech Min Sci 60:253-262. https://doi.org/10.1016/j.ijrmms.2012.12.004

[8] Hao T, Li F, Tang Y, Zhao L, Wang Z (2022) Infrared precursor of pre-cracked coal failure based on critical slowing down. Geomat Nat Hazards Risk 13(1):1682-1699. https://doi.org/10.1080/19475705.2022.2098068

[9] He M, Cheng T, Qiao Y, Li H (2023a) A review of rockburst: experiments, theories, and simulations. J Rock Mech Geotech Eng 15(5):1312-1353. https://doi.org/10.1016/j.jrmge.2022.07.014

[10] He Z, Xie Z, Zhang N, Han C, Xiang Z, Yan G, Qiao H, Shao C (2023b) Research on spatiotemporal evolution law of surrounding rock fractures and hierarchical collaborative control technology in high-stress soft rock roadway: a case study. Eng Fail Anal 150:107366. https://doi.org/10.1016/j.engfailanal.2023.107366

[11] Huang B, Wang P, Gao Y, Liu Q, Yuan W (2025) Experimental analysis of the failure modes and precursors of surrounding rocks in 3D-printed tunnels with rough fractures: insights into the influence of excavation shapes. Tunn Undergr Space Technol 160:106510. https://doi.org/10.1016/j.tust.2025.106510

[12] Kong B, Feng X, Sun X, Cao H, Zhang X, Yu S, Cao Z, Jia S (2025) Study on macroscopic and microscopic damage and evolution of coal rock based on acoustic emission time-varying characteristics. Bull Eng Geol Environ 84(2):75. https://doi.org/10.1007/s10064-024-04036-7

[13] Kong X, Zhan M, Cai Y, Ji P, He D, Zhao T, Hu J, Lin X (2023) Precursor signal identification and acoustic emission characteristics of coal fracture process subjected to uniaxial loading. Sustainability 15(15):11581. https://doi.org/10.3390/su151511581

[14] Lei R, Gu Q, Hu C, He P, Zhou L (2025) Acoustic emission signal characteristics and precursory recognition of rock failure in fractured sandstone. Rock Soil Mech

46(7):2023-2038. https://doi.org/10.16285/j.rsm.2024.1164
[15] Li J, Liu D, He M, Guo Y, Wang H (2023) Experimental investigation of true triaxial unloading rockburst precursors based on critical slowing-down theory. Bull Eng Geol Environ 82(3):65. https://doi.org/10.1007/s10064-023-03092-9
[16] Ling K, Liu D, Wang S, Guo Y, Zhang Y, Yang J, Zhang X (2025) Research on the synergetic precursors identification of rockburst based on the critical slowing-down theory and the Mann-Kendall test. Bull Eng Geol Environ 84(11):531. https://doi.org/10.1007/s10064-025-04549-9
[17] Ma J, Liu D, Zhang S, Du F, Hou Z, Jiang Z (2025) Study on critical power-law singularity of brittle creep failure in deep hole-containing sandstone. Geomech Geophys Geo-Energy Geo-Resour 11(1):107. https://doi.org/10.1007/s40948-025-01039-w
[18] Ma Z, Zuo J, Zhu F, Liu H, Xu C (2023) Non-orthogonal failure behavior of roadway surrounding rock subjected to deep complicated stress. Rock Mech Rock Eng 56(9):6261-6283. https://doi.org/10.1007/s00603-023-03397-x
[19] Niu Y, Zhou XP (2021) Forecast of time-of-instability in rocks under complex stress conditions using spatial precursory AE response rate. Int J Rock Mech Min Sci 147:104908. https://doi.org/10.1016/j.ijrmms.2021.104908
[20] Ren F, Tian Z, Ma K, Gu J (2025) Relationship between rock brittleness and rockburst early warning time. Int J Rock Mech Min Sci 195:106305. https://doi.org/10.1016/j.ijrmms.2025.106305
[21] Tang HD, Zhu ML (2020) Micro damage mechanics-based exponential power law acceleration of microscale damage and time-dependent crack propagation. Eng Fract Mech 229:106930. https://doi.org/10.1016/j.engfracmech.2020.106930
[22] Vasseur JRM, Wadsworth FB, Lavallée Y, Bell AF, Main IG, Dingwell DB (2015) Heterogeneity: the key to failure forecasting. Sci Rep 5(1):13259. https://doi.org/10.1038/srep13259
[23] Voight B (1988) A method for prediction of volcanic eruptions. Nature 332(6160):125-130. https://doi.org/10.1038/332125a0
[24] Wang CL, Zhou BK, Li CF, Wen ZJ, Bai ZA, Zhu CY, Sun L, Xue XH, Cao P (2024) Prediction and critical transition mechanism for granite fracture: insights from critical slowing down theory. J Cent South Univ 31(8):2748-2764. https://doi.org/10.1007/s11771-024-5707-3
[25] Wei Y, Li Z, Kong X, Zhang Z, Cheng F, Zheng X, Wang C (2018) The precursory information of acoustic emission during sandstone loading based on critical slowing down theory. J Geophys Eng 15(5):2150-2158. https://doi.org/10.1088/1742-2140/aac009
[26] Xie H, Gao M, Zhang R, Peng G, Wang W, Li A (2018) Study on the mechanical

properties and mechanical response of coal mining at 1000 m or deeper. Rock Mech Rock Eng 52(5):1475-1490. https://doi.org/10.1007/s00603-018-1509-y

[27] Xue J, Hao S, Wang J, Ke F, Lu C, Bai Y (2018) The changeable power law singularity and its application to prediction of catastrophic rupture in uniaxial compressive tests of geomedia. J Geophys Res Solid Earth 123(4):2645-2657. https://doi.org/10.1002/2018jb015591

[28] Yang H, Wang E, Wang X, Song Y, Chen D, Wang D, Li J (2024) Predicting the failure of rock using critical slowing down theory on acoustic emission characteristics. Eng Fail Anal 163:108474. https://doi.org/10.1016/j.engfailanal.2024.108474

[29] Zhai SF, Jiang YX, Zhang JZ (2021) Experimental investigations on progressive rupture and predictive acoustical behavior in brittle rocks. Arab J Geosci 14(13):1292. https://doi.org/10.1007/s12517-021-07676-1

[30] Zhang JZ, Zhou XP (2020) Forecasting catastrophic rupture in brittle rocks using precursory AE time series. J Geophys Res Solid Earth 125(8):e2019JB019276. https://doi.org/10.1029/2019jb019276

[31] Zhang JZ, Wu WT, Zhou XP (2023) On the predictability of localization instabilities of quasibrittle materials from accelerating rates of acoustic emission. Eng Fract Mech 289:109455. https://doi.org/10.1016/j.engfracmech.2023.109455

[32] Zhang L, Ren T, Li X, Tan L (2021a) Acoustic emission, damage and cracking evolution of complete coal under compressive loads: experimental and discrete element modelling. Eng Fract Mech 252:107690. https://doi.org/10.1016/j.engfracmech.2021.107690

[33] Zhang Q, Pei J, Liu Y, Li X, Nie B, Zhang J, Liu H (2025a) Study on the prediction method for coal and rock mass fracture process based on time series acoustic emission statistical model. Rock Mech Rock Eng 58(7):7631-7647. https://doi.org/10.1007/s00603-025-04524-6

[34] Zhang X, Liu J, Shi J (2025b) Critical slowing-down characteristics of acoustic emission during different rocks failure under uniaxial compression. J Saf Sci Technol 21(8):197-203.

[35] Zhang Z, Li Y, Hu L, Tang CA, Zheng H (2021b) Predicting rock failure with the critical slowing down theory. Eng Geol 280:105960. https://doi.org/10.1016/j.enggeo.2020.105960

[36] Zheng Y, Liu C, Lu K, Zhang H, Jian B, Zhang W (2025) Study on the fracture behavior and critical slowing down characteristics of saturated sandstone based on acoustic emission and resistivity. Sci Rep 15(1):12113. https://doi.org/10.1038/s41598-025-96072-w

[37] Zhou XP, Li CQ (2022) Prospective forecast of sliding instability time using a

precursory AE time series. Tribol Int 176:107887. https://doi.org/10.1016/j.triboint.2022.107887

[38] Zhu C, Huang M, Ren F, Li X, Gu J, Li H, He M (2025) Multivariate acoustic emissions precursors of rockburst from the perspective of early warning. Int J Min Sci Technol 35(5):703-717. https://doi.org/10.1016/j.ijmst.2025.04.002

[39] Zhu X, Tang Y, Fan J, Hu J, Liu J, He C (2022) Experimental study on failure precursors of fine sandstone based on critical slowing down theory. Chin J Rock Mech Eng 41(1):53-61. https://doi.org/10.13722/j.cnki.jrme.2021.0640